NANO LETTERS

2007
Vol. 7, No. 9
2655−2659

Gold-Catalyzed Oxide Nanopatterns for the Directed Assembly of Ge Island Arrays on Si

Jeremy T. Robinson,[†] Fulvio Ratto,[‡] Oussama Moutanabbir,[§,#] Stefan Heun,[||,⊗] Andrea Locatelli,[⊥] T. Onur Mentes,[⊥] Lucia Aballe,[⊥] and Oscar D. Dubon*[,†]

Department of Materials Science and Engineering, University of California, Berkeley, and Lawrence Berkeley National Laboratory, Berkeley, California 94720, INRS-EMT, Université du Québec, J3X 1S2 Varennes, Québec, Canada, Department of Applied Physics and Physico-Informatics, Keio University, Kouhoku-Ku, Yokohama 223-8522, Japan, CNR-INFM, Laboratorio Nazionale TASC, Basovizza, 34012 Trieste, Italy, and Sincrotrone Trieste S.C.p.A., Basovizza, 34012 Trieste, Italy

Received May 4, 2007; Revised Manuscript Received June 18, 2007

ABSTRACT

The heteroepitaxial growth of Ge on Au-patterned Si(001) is investigated using in situ spectromicroscopy. Patterning of a hydrogen-terminated Si surface with a square array of Au dots followed by brief exposure to air leads to the spontaneous, local oxidation of Si. The resulting oxide nanopattern limits the surface migration of Au during annealing up to 600 °C, resulting in complete preservation of the Au pattern. Subsequent deposition of Ge induces a redistribution of Au across the surface even as the oxide nanopattern persists. As a result, the oxide pattern drives the growth of Ge islands into an ordered assembly, while Au decorates the surfaces of the Ge islands and modifies their shape.

Metal/semiconductor interfaces have been widely investigated for the better part of a century.[1,2] Largely studied for their interesting electronic behavior, metals on semiconductors have more recently moved into the arena of semiconductor epitaxy.[3,4] In this context, metals modify nucleation and growth phenomena at the nanoscale. For example, metal overlayers have been exploited to tune the characteristics of epitaxial islands, or quantum dots (QDs), including their size, density, and to a limited extent, shape.[5,6] Additionally, metal films have been instrumental in catalyzing the growth of semiconductor nanowires[7] and nanotubes.[8,9]

Recently, Robinson et al. demonstrated that patterned metal overlayers enable the control over large areas of the position and shape of islands in the Ge on Si model heteroepitaxial system.[10−12] Germanium on Si grows via the Stranski−Krastanov (SK) mode, consisting of the formation of a wetting layer (WL) followed by the nucleation and growth of three-dimensional islands.[13−15] If the Si substrate is prepatterned with a square array of Au dots, the Ge islands assemble into a two-dimensional square lattice. These islands grow between the surface sites where the Au dots were deposited—henceforth referred to as "Au sites"—and have strikingly different shapes from islands that grow on Au-free Si.[10−12] Central to the ordering process is the existence of a barrier to Ge diffusion surrounding each Au site, which leads to the development of an island-free region, or denuded zone.[10] How the gold nanopattern gives rise to this diffusion barrier and affects the potential energy landscape on the surface is yet unknown. More generally, these observations raise fundamental questions concerning the physical and/or chemical contributions of patterned metal overlayers in semiconductor heteroepitaxial growth.

Here we present a spectromicroscopic investigation during the growth of ordered Ge islands on Au-patterned Si(001). In situ low-energy electron microscopy/diffraction (LEEM/LEED) and X-ray photoemission electron microscopy (XPEEM) of the growth surface provide direct insight into the interaction of patterned Au with both the Si substrate and Ge adsorbates. Annealing a square array of Au dots leaves the dot pattern unchanged; however, after Ge deposition, Au redistributes across the surface. The partial relocation of Au to the Ge islands modifies their growth and morphological evolution, while the presence of a spontaneously

* Corresponding author. E-mail: oddubon@berkeley.edu.
[†] Department of Materials Science and Engineering, University of California, Berkeley, and Lawrence Berkeley National Laboratory.
[‡] INRS-EMT, Université du Québec.
[§] Department of Applied Physics and Physico-Informatics, Keio University.
[||] CNR-INFM, Laboratorio Nazionale TASC.
[⊥] Sincrotrone Trieste S.C.p.A.
[#] Present address: Max-Planck Institute of Microstructure Physics, Halle D-06120, Germany.
[⊗] Present address: NEST CNR-INFM Scuola Normale Superiore, Piazza dei Cavalieri 7, 56126 Pisa, Italy.

10.1021/nl071051y CCC: $37.00
Published on Web 08/02/2007

formed oxide around each Au dot provides evidence for the possible origin of the aforementioned diffusion barrier.

Silicon (001) samples approximately 1×1 cm^2 and having a thickness of 380 ± 25 μm and resistivity of 1−10 Ω cm were rinsed in a dilute HF:H_2O (1:10) solution to remove the native oxide and hydrogen-terminate the surface. Following this, a silicon nitride stencil mask was placed directly in contact with the surface, and the sample was transferred to an electron-beam evaporation system. Nominally 1−2 nm of Au was deposited through the mask, which contains arrays of 200×200 nm^2 square windows with a range of pitches from 400 to 2000 nm. The total patterned area of the mask and substrate was 500×500 μm^2. After Au deposition, the mask was removed and the patterned sample was transferred in air to the SPELEEM microscope at the Nanospectroscopy beamline of the Elettra synchrotron facility where spectroscopic studies were carried out. Sample annealing and Ge growth were performed at sample temperatures between 450 and 600 °C. Germanium was deposited using a commercial molecular beam epitaxy (MBE) source at a rate of approximately 0.07 ML/min and base pressure of 3×10^{-10} Torr. The Ge coverages studied range from ~6 to 8 monolayers (ML) (1 ML of Ge = 6.27×10^{14} atoms/cm^2). In this range of coverages, islands on Au-patterned Si have a truncated pyramidal shape bound by {111} side facets, an average height between 50 and 70 nm (depending on the specific Ge coverage), and an aspect ratio in the range of 1:2 to 1:3 (height/base).[10] Samples were characterized in situ at various stages of preparation by LEEM, LEED, and XPEEM. The resolution of the instrument for imaging (10 nm for LEEM) and chemical mapping (30 nm for XPEEM) is very well suited for the dimensions of the structures and island patterns that are produced. In addition, the depth sensitivity of XPEEM is approximately 1 nm, which arises from the small mean free path (0.5 nm) of the excited photoelectrons in the solid.[16] Details of the LEEM/XPEEM setup and its use in similar growth experiments are described elsewhere.[17−21] Additional post-growth morphological characterization was completed via ex situ atomic force microscopy (AFM).

To map the chemical composition of the H-terminated, Au-patterned Si(001) surface, spectromicroscopy (XPEEM) was performed at the Si 2p and Au 4f core levels using a photon energy of 195 eV. Figure 1a presents spectra of the Si 2p core level from two different types of positions on the surface, as indicated in the XPEEM image inset. The binding energy (BE) scale in all spectra is referenced to the Au $4f_{7/2}$ core level emission at 84.5 eV.[22] The yellow (light) spectra were measured at locations away from the Au sites and are characterized by a single peak at approximately 99 eV BE. This peak is assigned to the Si 2p bulk component. In contrast, the blue (dark) spectra were taken at Au sites; in this case, two peaks appear at 99 and 103 eV BE. We attribute the peak at higher binding energy to oxidized Si, which is known to exhibit a peak approximately 4 eV higher than that corresponding to the Si 2p bulk component.[23] The measured Si 2p signal from within each Au site suggests that a small amount of Si has segregated to the surface, a

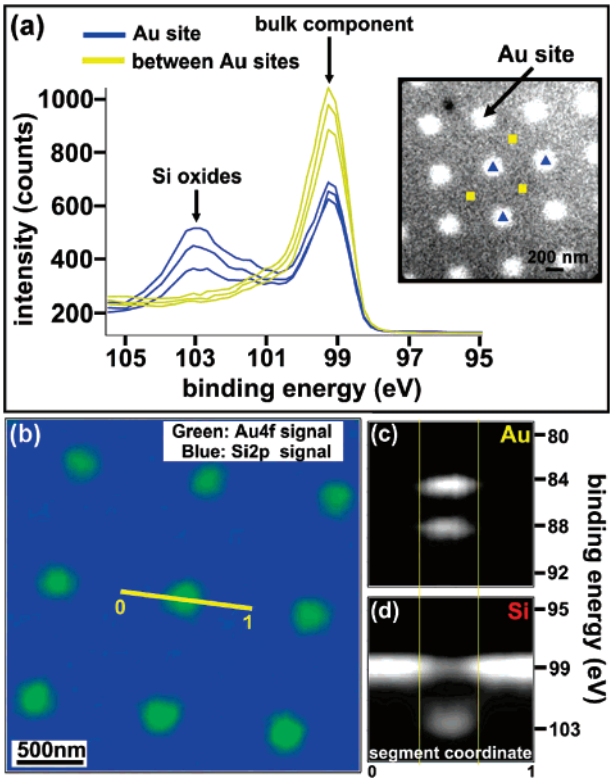

Figure 1. (a) Spectra of the Si 2p core level from an as deposited Au-patterned Si(001) sample. The yellow (light) curves show data collected away from the Au sites (shown in the XPEEM image inset as yellow squares) with a single peak at ~99 eV. The blue (dark) curves show data collected at the Au sites (blue triangles in inset), where a second peak arises around 103 eV. (b) Composite XPEEM image of Si 2p and Au 4f micrographs. The green (light) color shows the Au 4f signal, and the blue (dark) color shows the Si 2p signal. The line segment in (b) is used for alignment of the spectra presented in (c) and (d).

behavior that has been observed in studies of the Au-catalyzed oxidation of Si.[24] We note that the micro-LEED pattern of the Au-patterned surface is 1×1—expected from hydrogen-terminated Si(001)—and that no modification of the surface reconstruction due to the presence of the Au pattern was detected.

Parts b−d of Figure 1 display a composite micrograph and the Si 2p and Au 4f spectra from the H-terminated, Au-patterned Si(001) surface. The image in Figure 1b was prepared by combining the Si 2p and Au 4f micrographs. The bright-green spots indicate regions of high Au content, which is confined to the periodic sites where Au was deposited. The darker (blue) background denotes the dominant Si content due to the substrate. A strong correlation between the spatial positions of the Au 4f and Si oxide signal maxima is observed in the aligned spectra shown in Figure 1c,d. These observations are consistent with the ability of Au films to promote the oxidation of Si by the diffusion of Si through the Au film to the surface,[24] where it can react with air even at room temperature.[25,26] The formation of an alloyed Si−Au interlayer enhances Si oxidation by the Au-induced modification of the hybridization state of Si atoms.

A more significant observation perhaps is the persistence of the Si oxide peak in the immediate vicinity of each Au

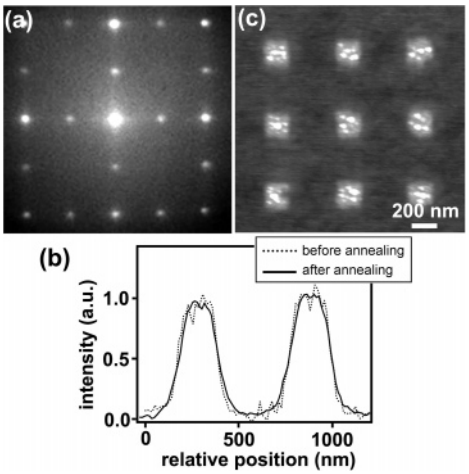

Figure 2. Spectroscopic and AFM analyses of Au-patterned regions characterized by a pitch of 600 nm for Au sites. (a) LEED pattern taken at energy of 53 eV in the Au-patterned region at 550 °C. The surface reconstruction has transitioned from a 1×1 structure to a superposition of the 1×2 and 2×1 reconstructions (double domain structure). (b) Cross-sectional intensity profiles of the Au 4f signal from a 600 nm pitch, Au-patterned region before and after annealing (different Au sites). The Au 4f signal before annealing shows slightly more noise due to a lower collection time. (c) AFM height image showing an Au-patterned sample after annealing. Several Au−Si solidified droplets are observed within each Au site. The height is truncated at 5 nm.

site. The XPEEM data as well as experiments concerning the wet chemical etching of Au-patterned Si[27] show that a robust oxide extends up to 100 nm beyond the perimeter of the Au sites; in effect, each Au site is bounded by an oxide corona, which forms electrochemically at the boundary between the Au site and the Si substrate. Removal of the Si native oxide by HF rinsing prior to Au deposition provides a conduction path for electrons between Si and Au and ensures that the electrochemical potential between them drives the local anodization of Si when exposed to air. We note that Si can be anodized locally in air that contains water vapor even without Au by applying an external potential, for example, with a scanning probe tip.[28]

To probe the thermal stability of the Au patterns on Si, samples were heated to 500−600 °C for 30 min and then quenched to room temperature. Characterization using LEEM and LEED was performed both at the annealing temperature and after quenching, while XPEEM was performed only after quenching due to the longer acquisition times. Figure 2a displays a micro-LEED pattern acquired during annealing at 550 °C from a region patterned with Au. The area sampled was 2×2 μm^2, which includes about ten Au sites. The pattern is a superposition of the 1×2 and 2×1 reconstruction domains—well-known from clean Si(001) surfaces—resulting from the desorption of hydrogen. Surface reconstructions associated with a Au-decorated surface were not observed.[29,30]

Figure 2b shows a direct comparison of Au 4f signals from an as-prepared and an annealed, Au-patterned sample. The line profiles across two Au sites match each other very well, demonstrating that thermal annealing alone does not result in a loss or smearing of the Au pattern. Additional ex situ

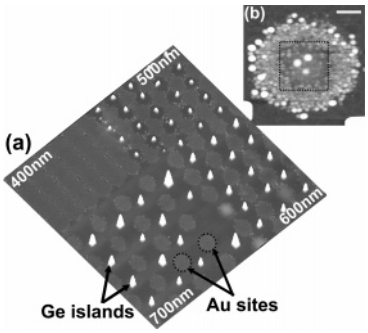

Figure 3. (a) Perspective AFM height image showing the intersection of four Au-patterned regions of different Au-site spacing (Image size: 5×5 μm^2; $z = 100$ nm). The Au-pattern pitch increases clockwise from 400 to 700 nm as indicated. (b) AFM height image of a representative Au site after Ge deposition (Scale bar in upper right corner = 100 nm; $z = 5$ nm). Small Ge islands with average height of 3.5 nm and width of 15 nm are agglomerated around the Au site. The image was taken from a sample grown in a conventional molecular beam epitaxy reactor as described in ref 10. The dotted square outlines the approximate boundary of the original Au site.

atomic force microscopy (AFM) shows that the square footprint is retained with several solidified droplets within each site (Figure 2c). Above approximately 360 °C, Au and Si form a liquid eutectic alloy whose composition follows the Si-rich liquidus line of the Au−Si phase diagram as the temperature is increased. Upon cooling to below this eutectic temperature, the molten alloy solidifies into the observed droplets within the square footprint of the Au sites. The preservation of the Au pattern upon annealing is a direct consequence of the existence of an oxide that inhibits the diffusion of Au, which is a well-known, fast diffusing species on the Si surface.[31] Our observations are in agreement with recent experiments indicating that the Au-catalyzed oxidation of the surface of a Si nanowire restricts the diffusion of Au away from the (Au) catalyst droplet during nanowire synthesis by the vapor−liquid−solid process.[32]

The characteristics of Ge island growth observed at the Nanospectroscopy beamline are consistent with those of earlier investigations.[10] Figure 3a shows a perspective AFM height image taken at the intersection of four Au-patterned regions, each characterized by a particular Au-site spacing, after deposition of nominally 8 ML of Ge at 450 °C. The Ge islands, which appear as tall, ordered pyramids in Figure 3a, have grown between the Au sites. Although the deposition rate and temperature here are 2 orders of magnitude and 150 °C lower, respectively, than in previous reports,[10−12] island shape and ordering are similar, demonstrating that Ge islands can be assembled on Au-patterned Si over a wide range of growth conditions. Figure 3b shows a single Au site after Ge deposition.

We now turn to the compositional evolution of the growth surface. Concentration maps obtained by XPEEM on the Ge 3d, Si 2p, and Au 4f core levels after the deposition of Ge on Au-patterned Si are shown in Figure 4. The formation of a nonuniform Ge wetting layer that contains a periodic array of depleted annular regions centered at the Au sites is demonstrated in Figure 4a. These regions appear as dark rings

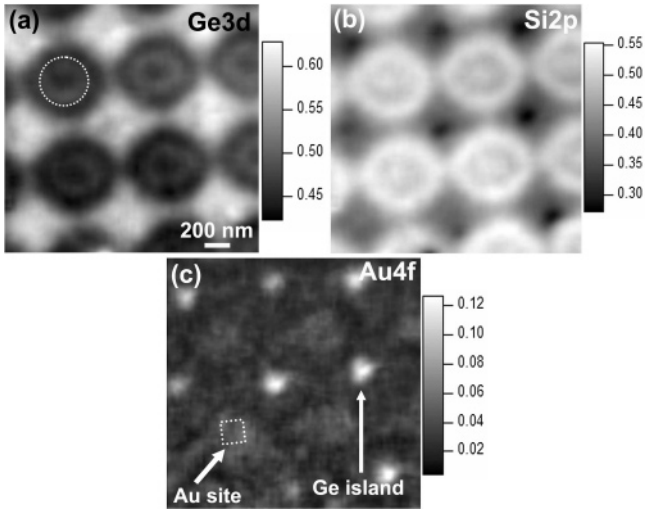

Figure 4. XPEEM-derived concentration maps obtained after Ge deposition in a Au-pattern region (pitch of 700 nm) for (a) Ge, (b) Si, and (c) Au energies. These maps were compiled using an analytical technique developed by Ratto et al.[17,18] All images are taken at the same position. The scale bar in (a) applies to (b) and (c).

that correspond to the Ge denuded zones and are bounded by smaller rings of higher Ge concentration (one of them is indicated by the dotted circle in Figure 4a). The bright rings consist of clusters of small Ge islands that grow directly around the square footprint of the Au sites and extend 100−150 nm beyond the Au site perimeter as seen in Figure 3b. The clusters appear in Figure 3 as nearly circular patches centered at the Au sites. We note that, as the pitch of the gold pattern decreases to 400 nm, these small Ge clusters cover a majority of the growth surface and inhibit the growth of the larger ordered islands (quadrant labeled "400 nm" in Figure 3a). The map of the Si content is approximately the converse of that of Ge content (Figure 4b). For example, the bright rings associated with a large Si signal are positioned where the Ge signal is weakest. In addition, the Ge islands appear as dark spots because they block electron emission from the underlying Si (thus attenuating the Si signal).

The deposition of Ge results in a dramatic transformation of the Au pattern as seen by the composition variation in Figure 4c. Traces of Au are still found at the sites where it was deposited; however, now Au is nonuniformly distributed across the patterned region—a 125 × 125 μm^2 area that includes $\sim 10^4$ Au sites. This marked enhancement of Au diffusion is perhaps due to the formation of a Ge layer or a Au−Ge−Si eutectic liquid that extends over the oxide corona and enables Au to migrate. The strongest signal from surface Au is measured precisely at the sites where the Ge islands have formed. This result in combination with an analysis of the effect of patterned metal species on island morphology[12] demonstrates that the unique shapes that Ge islands assume in the Au-patterned regions are at least in part caused by Au. Metals are known to modify the free energy of semiconductor surfaces and to influence the shape of heteroepitaxial islands.[4]

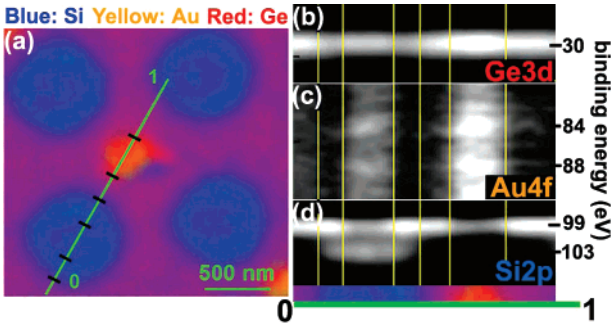

Figure 5. (a) Concentration map of the Ge, Si, and Au micrographs. The Au site spacing in this case is 1000 nm. Spatially aligned Ge 3d, Au 4f, and Si 2p spectra along the line segment in (a) are shown in (b), (c), and (d), respectively. The ticks along the line segment in (a) are indicated as vertical lines in the aligned spectra. A spatially aligned strip from the composite image along the line segment is also presented for reference.

The effect of Ge on the composition of the growth surface is best illustrated in Figure 5a, which presents a composite composition map obtained from Ge 3d, Au 4f, and Si 2p micrographs. Each of the four circular (blue) regions consists of a Au site and its associated Ge denuded zone. The strongest Ge 3d and Au 4f signals (also illustrated in parts b and c of Figure 5, respectively) are spatially co-incident and located away from the Au sites. Most importantly, the Si 2p spectra in Figure 5d clearly show *both* the bulk Si and Si oxidation states peaked at 99 and 103 eV, respectively. The Si oxide signal is highest at the Au site and decreases monotonically across the Ge denuded zone. In this case, the aligned spectra reveal a direct spatial correspondence between the Au-catalyzed Si oxide and the Ge denuded zone.

These experiments demonstrate the remarkable effect of Au patterns on Si. Upon exposure to air, Au catalyzes the oxidation of Si. The resulting oxide nanopattern blocks Ge adatoms outside the oxide coronae from diffusing toward the Au sites, resulting in the formation of the Ge denuded zones; in effect, the oxide forms a diffusion barrier in a manner consistent with kinetic Monte Carlo simulations.[10] Enhanced accumulation of Ge away from the Au sites enables island nucleation even at nominal Ge coverages as low as 1.5 ML, which is below the critical wetting-layer thickness for islanding in the metal-free regions of the sample.[10,11] Uncovering this complex growth behavior provides a conceptual framework for understanding metal-mediated growth phenomena in semiconductor nanostructure synthesis by physical vapor processes.

Acknowledgment. We thank F. M. Ross for fruitful discussions on Au-induced oxidation, J. A. Liddle for stencil mask fabrication, M. Tonezzer from Laboratorio Nazionale TASC CNR-INFM for technical support in preparing Au-patterned Si samples, Dr. F. Cicoira (INRS) for a critical reading of the manuscript and M. Seibt for fruitful discussions on Au−Ge−Si eutectics. O. D. Dubon acknowledges support from NSF under contract no. DMR-0349257. J. T. Robinson acknowledges support from the IBM Ph.D. fellowship program. O. Moutanabbir is grateful to K. M. Itoh and to JSPS for their support. F. Ratto is grateful to DEST (Australia) and FQRNT for graduate fellowship support.

References

(1) Frenkel, J.; Joffé, A. *Phys. Rev.* **1932**, *39*, 530.
(2) Fan, H. Y. *Phys. Rev.* **1942**, *62*, 388.
(3) Wagner, R. S.; Ellis, W. C. *Appl. Phys. Lett.* **1964**, *4*, 89.
(4) Copel, M.; Reuter, M. C.; Kaxiras, E.; Tromp, R. M. *Phys. Rev. Lett.* **1989**, *63*, 632.
(5) Berbezier, I.; Ronda, A.; Portavoce, A.; Motta, N. *Appl. Phys. Lett.* **2003**, *83*, 4833.
(6) Eaglesham, D. J.; Unterwald, F. C.; Jacobson, D. C. *Phys. Rev. Lett.* **1993**, *70*, 966.
(7) Fan, H. J.; Werner, P.; Zacharias, M. *Small* **2006**, *2*, 700 and references therein.
(8) Li, Y. B.; Bando, Y.; Golberg, D. *Adv. Mater.* **2004**, *16*, 37.
(9) Goldberger, J.; He, R. R.; Zhang, Y. F.; Lee, S. W.; Yan, H. Q.; Choi, H. J.; Yang, P. D. *Nature* **2003**, *422*, 599.
(10) Robinson, J. T.; Liddle, J. A.; Minor, A.; Radmilovic, V.; Yi, D. O.; Greaney, P. A.; Long, K. N.; Chrzan, D. C.; Dubon, O. D. *Nano Lett.* **2005**, *5*, 2070.
(11) Robinson, J. T.; Liddle, J. A.; Minor, A.; Radmilovic, V.; Dubon, O. D. *J. Cryst. Growth* **2006**, *287*, 518.
(12) Robinson, J. T.; Walko, D. W.; Arms, D. A.; Tinberg, D. S.; Evans, P. G.; Cao, Y.; Liddle, J. A.; Rastelli, A.; Schmidt, O. G; Dubon, O. D. *Phys. Rev. Lett.* **2007**, *98*, 106102.
(13) Medeiros-Ribeiro, G.; Bratkovski, A. M.; Kamins, T. I.; Ohlberg, D. A. A.; Williams, R. S. *Science* **1998**, *279*, 353.
(14) Ross, F. M.; Tromp, R. M.; Reuter, M. C. *Science* **1999**, *286*, 1931.
(15) Stangl, J.; Holý, V.; Bauer, G. *Rev. Mod. Phys.* **2004**, *76*, 725 and references therein.
(16) Seah, M. P.; Dench, W. A. *Surf. Interface Anal.* **1979**, *1*, 2.
(17) Ratto, F.; Rosei, F.; Locatelli, A.; Cherifi, S.; Fontana, S.; Heun, S.; Szkutnik, P.-D.; Sgarlata, A.; Crescenzi, M. D.; Motta, N. *J. Appl. Phys.* **2005**, *97*, 043516.
(18) Ratto, F.; Locatelli, A.; Fontana, S.; Kharrazi, S.; Ashtaputre, S.; Kulkarni, S. K.; Heun, S.; Rosei, F. *Small* **2006**, *2*, 401.
(19) Locatelli, A.; Aballe, L.; Mentes, T. O.; Kiskinova, M.; Bauer, E. *Surf. Interface Anal.* **2006**, *38*, 1554.
(20) Heun, S.; Watanabe, Y.; Ressel, B.; Bottomley, D.; Schmidt, Th.; Prince, K. C. *Phys. Rev. B* **2001**, *63*, 125335.
(21) Biasiol, G.; Heun, S.; Golinelli, G. B.; Locatelli, A.; Mentes, T. O.; Guo, F. Z.; Hofer, C.; Teichert, C.; Sorba, L. *Appl. Phys. Lett.* **2005**, *87*, 223106.
(22) Haruyama, Y.; Kanda, K.; Matsui, S. *J. Electron Spectrosc.* **2005**, *144*−*147*, 389.
(23) Himpsel, F. J.; McFeely, F. R.; Taleb-Ibrahimi, A.; Yarmoff, J. A. *Phys. Rev. B* **1988**, *38*, 6084.
(24) Hiraki, A.; Nicolet, M. A.; Mayer, J. W. *Appl. Phys. Lett.* **1971**, *18*, 178.
(25) Cros, A.; Derrien, J.; Salvan, F. *Surf. Sci.* **1981**, *110*, 471.
(26) Derrien, J.; Cohen, C.; Cros, A.; Layet, J. M.; Salvan, F.; Abel, F.; Boulliard, J. C.; Domange, J. L.; Sotto, M. *Appl. Phys. Lett.* **1981**, *39*, 915.
(27) Robinson, J. T.; Evans, P. G.; Liddle, J. A.; Dubon, O. D. *Nano Lett.* **2007**, *7*, 2009.
(28) Dagata, J. A.; Scneir, J.; Harary, H. H.; Evans, C. J.; Postek, M. T. Bennett, J. *Appl. Phys. Lett.* **1990**, *56*, 2001.
(29) Kageshima, M.; Torii, Y.; Tano, Y.; Takeuchi, O.; Kawazu, A. *Surf. Sci.* **2001**, *472*, 51.
(30) Lin, X. F.; Wan, K. J.; Glueckstein, J. C.; Nogami, J. *Phys. Rev. B* **1993**, *47*, 3671.
(31) Hannon, J. B.; Kodambaka, S.; Ross, F. M.; Tromp, R. M. *Nature* **2006,** *440*, 69.
(32) Kodambaka, S.; Hannon, J. B.; Tromp, R. M.; Ross, F. M. *Nano Lett.* **2006**, *6*, 1292.

NL071051Y